






A 1500-year record of mercury isotopes in seal feces documents sea ice changes in the Antarctic

Hongwei Liu¹, Wang Zheng ^{2,3} , Bridget A. Bergquist³, Yuesong Gao¹, Fange Yue¹, Lianjiao Yang¹, Liguang Sun¹ & Zhouqing Xie ¹ 

Temporal and spatial variations in sea ice coverage at high Northern Hemisphere latitudes have been shown to affect the photodegradation of methylmercury in seawater and the mercury isotope signatures in biological samples, suggesting the potential of mercury isotopes to reconstruct sea ice variability. Here we study the mercury isotopic composition of a 1500-year sediment profile strongly affected by seal activities on the Fildes Peninsula, King George Island, Antarctic Peninsula. The mass independent isotope fractionation of mercury (represented by $\Delta^{199}\text{Hg}$) in sediments dominated by seal feces input reflects the $\Delta^{199}\text{Hg}$ of marine methylmercury before entering the food web, documenting the changes in the degree of photodemethylation. We found much higher $\Delta^{199}\text{Hg}$ in sediments deposited during a warm period (~700-1000 years ago), suggesting that reduced sea ice promoted greater photodemethylation. Thus, this study demonstrates the modulation of methylmercury photodegradation by sea ice in the Antarctic, and that mercury isotopes can record historical sea ice changes.

¹ Department of Environmental Science and Engineering, Anhui Key Laboratory of Polar Environment and Global Change, University of Science and Technology of China, Hefei, Anhui 230026, China. ² Institute of Surface-Earth System Science, School of Earth System Science, Tianjin University, Tianjin 300072, China.

³ Department of Earth Sciences, University of Toronto, 22 Ursula Franklin Street, Toronto, ON M5S 3B1, Canada. email: zhengw3@tju.edu.cn; zqxie@ustc.edu.cn

As a global pollutant, mercury (Hg) can be transported over long distances in the atmosphere, reaching even the most remote locations including the polar regions¹. Thus elevated Hg levels have been observed in the Antarctic and the Southern Ocean^{2,3}. Following deposition of Hg to oceans, a fraction of Hg is reduced and re-emitted into the atmosphere^{4–6}. The remaining Hg can be converted to methylmercury (MeHg)^{7–10}, which is highly toxic and highly bioavailable. MeHg may then enter the food chain, posing a threat to marine organisms, especially marine predators. For example, high Hg levels up to 73.4 $\mu\text{g g}^{-1}$ have been reported in the feathers of long-lived birds in the Southern Ocean¹¹.

In the oceanic photic zone, MeHg undergoes photodegradation, contributing to the observed low MeHg concentration in surface seawater^{2,12–14}. Therefore, photodemethylation is considered to be an important sink for MeHg in the upper ocean^{13,15,16}. Evidence suggests that many factors can affect the photodemethylation of MeHg, such as light intensity, salinity, dissolved organic matter, etc., among which sunlight plays a dominant role^{15–19}. Interestingly, previous studies suggest that the extent and concentration of sea ice at high Northern Hemisphere latitudes can cause changes in the photodegradation of MeHg by altering the amount of solar radiation that penetrates the seawater^{20,21}. However, this phenomenon has not been demonstrated in the Antarctic and further research is needed.

The past two decades have seen Hg isotopes emerging as a powerful tool for tracing the sources and pathways of Hg in the environment²². Mercury isotopes exhibit mass-dependent fractionation (MDF, represented by $\delta^{202}\text{Hg}$) during almost all biotic and abiotic chemical reactions²³. In contrast, large magnitude mass-independent fractionation (MIF) for odd-mass-number isotopes (odd-MIF, $\Delta^{199}\text{Hg}$ and $\Delta^{201}\text{Hg}$) only occurs in photochemical reactions^{23,24}. For example, both the photoreduction of inorganic Hg(II) and photodemethylation of MeHg in the aqueous phase with the presence of dissolved organic matter enrich odd isotopes in the residual Hg(II) or MeHg^{23,24}. The odd-MIF produced in aqueous photochemical reactions may be transferred to aquatic organism due to the absence of Hg MIF during trophic transfer and metabolism^{20,21,25–27}. Thus, the Hg MIF values in biological tissues allow us to study the photochemical processes experienced by Hg before entering the food web. Both Point et al.²¹ and Masbou et al.²⁰ used Hg MIF values in biological samples (i.e., seabird eggs and ringed seal tissues) to infer changes in the degree of photodemethylation in seawater and found a strong control of MeHg photodegradation by sea ice. Zheng et al.²⁸ found evidence for enhanced photodemethylation during the Little Ice Age based on the odd-MIF of Hg in Antarctic biological sediments, which was proposed to link to the enlargement of polynyas (open water within sea ice). Therefore, the effect of sea ice change on marine MeHg cycle is well-captured by Hg isotope compositions in biological samples, indicating that Hg isotopes are a promising indicator of sea ice change.

The Antarctic Peninsula is one of the most rapidly warming regions on Earth, with an observed maximum rate of $\sim 0.5^\circ\text{C}$ per decade since 1950²⁹, although some studies suggest that this warming has momentarily declined or that a cooling has been occurring since the late 1990s^{30–32}. Higher temperatures are accompanied by rapid changes in the cryosphere and ecosystems of the Antarctic Peninsula, such as: (1) accelerated disintegration of glaciers, with about 52% of the glaciers showing retreat and only about 9% advancing during 1991–2015³³; (2) reduction in seasonal sea ice extent, with the extent of summer sea ice in the Weddell Sea dropping to a near-record level in the satellite era in 2016/17^{34–36}. This rapid climate change is expected to strongly affect the Hg cycle in the Antarctic Peninsula region. The ice-free areas of the Antarctic Peninsula are home to Southern Ocean

predators such as penguins and seals, and the biological sediments produced by their activities provide unique archives for studying past climate change and the Antarctic Hg cycle^{37,38}.

In this study we report the Hg isotope compositions of a sediment core (HF4) strongly influenced by seal feces on the Fildes Peninsula, King George Island, Antarctic Peninsula (Fig. 1 and Supplementary Fig. 1)^{39,40}. The objects of this study are to identify the source of Hg and to reconstruct past changes in the degree of photodemethylation and its relationship to climate change (such as changes in sea ice coverage). We show that the source of Hg in the sediment after ~ 470 CE was dominated by Hg input from seal feces. In particular, changes in $\Delta^{199}\text{Hg}$ in sediments after ~ 750 CE recorded changes in the degree of photodemethylation in the ocean, which was strongly controlled by changes in sea ice.

Results and discussion

Sources of Hg to the sediments. Large amounts of seal hair were found in sediment samples above 23 cm depth (Fig. 2). The number of seal hairs varies from 0.18 g^{-1} to 3734 g^{-1} , with an average of $1359 \pm 1059 \text{ g}^{-1}$ (1 SD, $n = 38$), indicating that the HF4 sedimentary column is strongly influenced by the input of seal remnants (i.e., seal hairs and feces)^{39,40}. According to modern surveys, the main seal species inhabiting the vicinity of our study site are southern elephant seals (*Mirounga leonina*) and Weddell seals (*Leptonychotes weddellii*)⁴¹. Our sediment core is likely primarily affected by southern elephant seal activity, since this species is dominant in Fildes Peninsula (maximum count ~ 1383 , against ~ 123 for Weddell seals)⁴². Sun et al.³⁹ reconstructed seal population changes over the past ~ 1500 years based on the number of seal hairs in HF4 sediments. Seal populations remained low until ~ 470 CE, followed by an obvious increase, reaching the first peak at ~ 750 CE (Fig. 2). Subsequently, seal populations declined markedly, reaching a minimum at ~ 1000 CE. From ~ 1000 to ~ 1300 CE, there was again a notable increase in seal populations. From ~ 1300 to ~ 1800 CE, the seal populations decreased first, and then increased to a certain extent. After ~ 1800 CE, seal populations appeared to decline again. The Hg content in sediments shows a trend consistent with the number of seal hairs (Pearson's $r = 0.66$, two-sided t test with p value < 0.001 , $n = 38$; Fig. 2 and Supplementary Fig. 2). Before ~ 470 CE, the Hg content in the sediments was relatively low, with an average value of $20.2 \pm 6.0 \text{ ng g}^{-1}$ (1 SD, $n = 14$). After ~ 470 CE, synchronizing with the increase of seal population, the Hg level in the sediments increased to an average of $203.0 \pm 80.4 \text{ ng g}^{-1}$ (1 SD, $n = 34$), much exceeding the soil background value in the Fildes Peninsula ($< 13 \text{ ng g}^{-1}$)⁴³. In the following discussion, we further explore the source of Hg to sediments using Hg isotopes.

Post-depositional alterations on the Hg isotope signatures in biological sediments are likely negligible, because as previously proposed, Hg in sediments is strongly bound to organic matter and minerals, limiting its mobility and reactivity^{23,28,44–47}. Therefore, it is reasonable to assume that Hg isotope signals in sediments reflect those of Hg sources. The $\delta^{202}\text{Hg}$ and $\Delta^{199}\text{Hg}$ exhibit large variations throughout the HF4 core, whereas $\Delta^{200}\text{Hg}$ is always near zero with no noticeable variation (Fig. 2 and Supplementary Table 1). Thus, the following discussion will be focusing on $\delta^{202}\text{Hg}$ and $\Delta^{199}\text{Hg}$. Overall, the variation of Hg isotopes can be divided into two periods. Before ~ 470 CE (hereinafter referred to as period I), $\delta^{202}\text{Hg}$ and $\Delta^{199}\text{Hg}$ were relatively low, with average values of $-0.76 \pm 0.19\text{‰}$ (1 SD, $n = 10$) for $\delta^{202}\text{Hg}$ and $0.12 \pm 0.11\text{‰}$ for $\Delta^{199}\text{Hg}$ (Fig. 3b), which are both similar to those of geogenic Hg within error^{23,48}. The slightly positive $\Delta^{199}\text{Hg}$ during period I is also similar to marine sediments receiving primarily background atmospheric Hg deposition (meaning atmospheric Hg that has undergone long-range transport

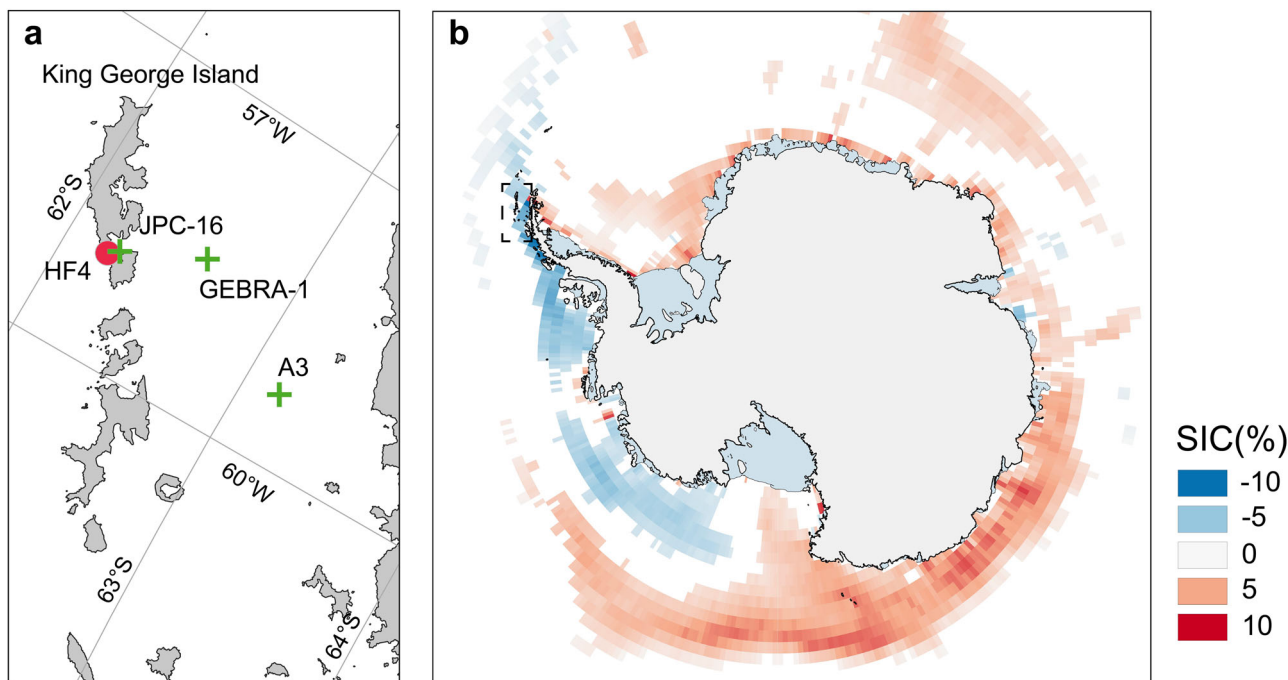


Fig. 1 Location of sampling sites in the Antarctic Peninsula and trends in sea ice concentration in the Antarctic region. **a** The location of the sampling sites. The red filled circle represents the sediment core HF4 in this study, and the green plus signs represent the JPC-16⁷², GEBRA-1¹⁰³ and A3¹⁰⁴ sediment cores from previous studies. **b** Trends of sea ice concentration¹⁰² (SIC; red-blue shading surrounding the continent; % per decade) are calculated over 1979–2020. The trends in sea ice concentration plotted in the figure all pass the two-sided *t* test with a significance level of 0.1. The dotted rectangular box in subpanel (**b**) represents the geographic extent of subpanel (**a**).

and been well mixed) in non-polar regions^{27,49,50}. Moreover, sediments in period I also show the lowest Hg contents that are close to the local soil background value⁴³, the lowest seal population and extremely low loss on ignition and phosphorous content (indicators of biological inputs) (Supplementary Fig. 3)^{39,40}. Taken together, Hg in sediments during period I was most likely sourced from bedrock weathering and additional contribution from background atmospheric deposition, but the input from biological remnants such as seal feces was likely minor.

After ~470 CE (hereinafter referred to as period II), both $\delta^{202}\text{Hg}$ and $\Delta^{199}\text{Hg}$ increased markedly, reaching $1.79 \pm 0.24\%$ (1 SD, $n = 14$) and $1.75 \pm 0.19\%$, respectively. The positive $\Delta^{199}\text{Hg}$ values of sediments during period II are significantly different from those of atmospheric aerosols in the Antarctic^{51–53}, polar snow^{45,53,54}, volcanic emission^{55–57}, terrestrial vegetation^{58–60}, and soil/bedrock weathering products^{61–63} (two-sided *t* test, all *p* values $\ll 0.01$), which have either near-zero or negative $\Delta^{199}\text{Hg}$ (Fig. 3a), suggesting negligible inputs from these sources. Moreover, background atmospheric deposition is also unlikely the dominant Hg source during period II because the Hg concentration of sediments during this period ($203.0 \pm 80.4 \text{ ng g}^{-1}$) is much higher than that in nearby sediments dominated by atmospheric deposition in the Fildes Peninsula ($\sim 2.5 \text{ ng g}^{-1}$)⁴³, indicating that the low atmospheric deposition flux could not explain the high Hg accumulation in sediments. Instead, the strongly positive $\Delta^{199}\text{Hg}$ values during period II are more similar to those of seal-feces-dominated sediments and modern seal feces in other regions of Antarctica²⁸ (Fig. 3b). Therefore, the source of Hg to sediments during period II was likely dominated by the input of seal feces, as evidenced by the relatively high seal population during this period.

While seal feces input was the dominant source of Hg in sediments during period II, the variations of $\Delta^{199}\text{Hg}$ and seal populations were not completely synchronized (Fig. 2). The Hg content and $\Delta^{199}\text{Hg}$ values in sediments were elevated alongside

the increase of seal population from ~470 to ~750 CE, suggesting that the increased Hg input from seal feces led to the increase of $\Delta^{199}\text{Hg}$ during this time interval. However, during the period from ~750 to ~1300 CE, seal populations and Hg concentrations in sediments first decreased and then increased, but $\Delta^{199}\text{Hg}$ showed an opposite trend, with a distinct peak corresponding to a decline in seal population. After ~1300 CE, although seal population and Hg content of sediments still showed large fluctuations, the $\Delta^{199}\text{Hg}$ values showed no obvious variation. Therefore, the variation of $\Delta^{199}\text{Hg}$ after ~750 CE cannot be explained by the change in the fraction of seal feces input to sediments. We suggest that the change in $\Delta^{199}\text{Hg}$ after ~750 CE is more likely attributable to the change in $\Delta^{199}\text{Hg}$ of seal feces themselves, which reflects the $\Delta^{199}\text{Hg}$ of Hg ingested by seals. Below we further discuss the possible causes of the $\Delta^{199}\text{Hg}$ variation in sediments dominated by seal feces.

The cause of the $\Delta^{199}\text{Hg}$ variation in seal-feces-dominated sediments. Since trophic transfer and biological metabolism are generally found to not produce Hg MIF^{21,64–66}, the $\Delta^{199}\text{Hg}$ of seal feces should mainly reflect the $\Delta^{199}\text{Hg}$ characteristics in the prey of seals. Thus, the variation of $\Delta^{199}\text{Hg}$ in seal-feces-dominated sediments after ~750 CE should reflect changes in either (1) the predatory feeding behavior of seals over the historical period, or (2) the $\Delta^{199}\text{Hg}$ at the base of the marine food chain.

The change in the predatory feeding behavior of seals over the historical period is unlikely the main cause of the $\Delta^{199}\text{Hg}$ variation. Previous studies have shown that marine organisms living at deeper depths generally have lower $\Delta^{199}\text{Hg}$, because the degree of the photodegradation of MeHg prior to uptake into the food web decreases with depth in the ocean^{25,67}. For example, the $\Delta^{199}\text{Hg}$ of pilot whales in mesopelagic waters is much lower than the $\Delta^{199}\text{Hg}$ of fish feeding in upper waters, but close to the $\Delta^{199}\text{Hg}$ of fish

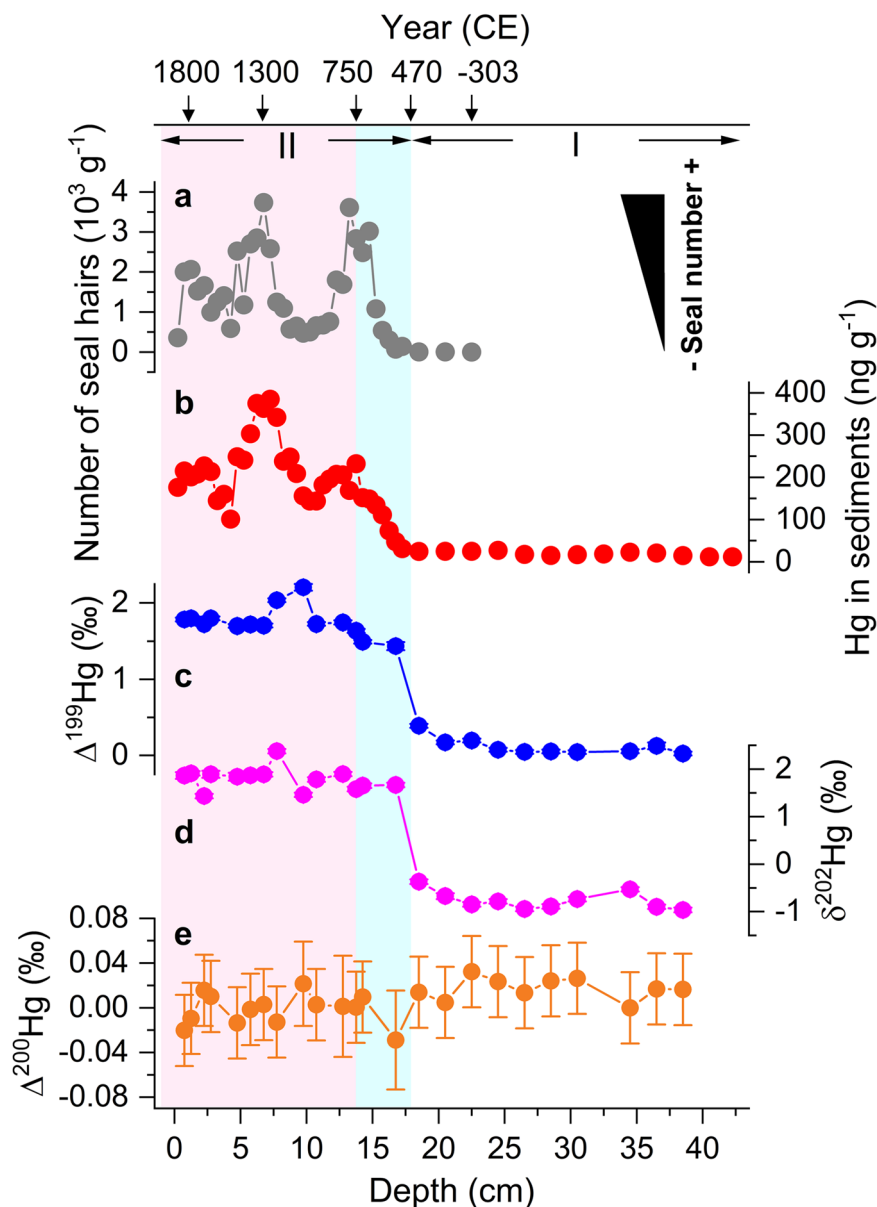


Fig. 2 The number of seal hairs, Hg concentration and Hg isotopes in the HF4 sediment column. **a** Changes in seal hair numbers in the sediments, indicating changes in seal populations over historical periods. Variations of Hg concentration (**b**), $\Delta^{199}\text{Hg}$ (**c**), $\delta^{202}\text{Hg}$ (**d**), and $\Delta^{200}\text{Hg}$ (**e**) in the HF4 sediments. Error bars for $\Delta^{199}\text{Hg}$, $\delta^{202}\text{Hg}$, and $\Delta^{200}\text{Hg}$ represent analytical uncertainty (2σ , see Methods for details). The Roman numerals represent different periods.

feeding in deeper waters^{25,68} (Fig. 3b). Therefore, predation depth could strongly affect $\Delta^{199}\text{Hg}$. Multiple lines of evidence suggest that Fildes Peninsula has experienced alternating warm and cold periods over the past 2,000 years, such as Medieval Climate Anomalies (MCA, from ~1000 CE to ~1300 CE) and the Little Ice Age (LIA, from ~1300 CE to ~1750 CE) (Fig. 4)^{69–76}. To adapt to this climate change, the predation depth of seals may have changed accordingly. McIntyre et al.⁷⁷ demonstrated that elephant seals tend to dive to deeper depths when foraging in warmer waters, possibly because the vertical distribution of prey is linked to water temperature. The period from ~1000 CE to ~1300 CE was a period of warm climate, which should have been characterized by warmer waters and reduced sea ice in the study area (Fig. 4). Increased water temperature and light entering the ocean due to reduced sea ice have been found to promote deeper predation for seals^{77,78}. The deepening of the predation depth is expected to lower the $\Delta^{199}\text{Hg}$ in seals, and eventually lead to the decrease in the $\Delta^{199}\text{Hg}$

of sediments, which is contradictory to the higher $\Delta^{199}\text{Hg}$ in sediments during this time interval (Fig. 4). Conversely, ~750–1000 CE and ~1300–1750 CE were periods of colder climates, which should have been accompanied by lower sea temperature and more sea ice, so the predation depth of seals should have been shallower, also inconsistent with the lower $\Delta^{199}\text{Hg}$ in sediments during these two periods. Therefore, we argue that the change in seal predation depth is not the main cause of $\Delta^{199}\text{Hg}$ variation after ~750 CE.

Thus, we hypothesize that the variation of $\Delta^{199}\text{Hg}$ in seal-feces-dominated sediments reflects the change of $\Delta^{199}\text{Hg}$ at the base of the marine food chain, which is eventually traced back to the $\Delta^{199}\text{Hg}$ produced by photochemical processes in seawater. Both the photoreduction of inorganic Hg(II) and the photodegradation of MeHg produce $\Delta^{199}\text{Hg}$ ^{23,24}. However, we argue that the MeHg photodegradation is the main process contributing to the $\Delta^{199}\text{Hg}$ variation in seal-feces-dominated sediments, whereas the inorganic Hg(II) photoreduction is likely a minor

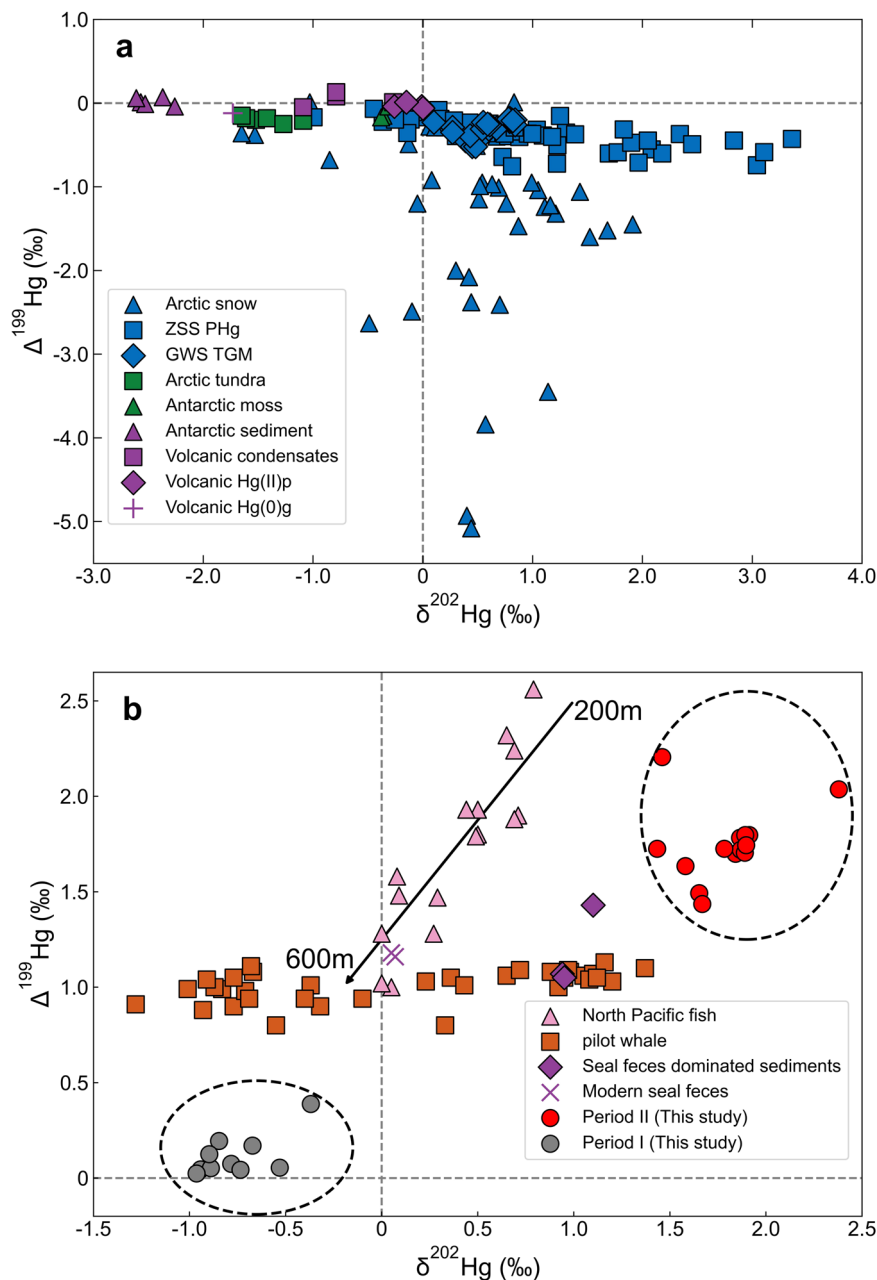


Fig. 3 Hg isotope compositions of different natural samples. a Hg isotope signatures of potential non-seal fecal sources (snow, atmospheric deposition, plants, bedrock weathering, volcanic emissions) to the sediments. **b** Hg isotope compositions of marine biological samples, seal feces, seal feces-dominated sediments, and the HF4 sediments in this study. The gray-filled circles in subpanel (b) represent the Hg isotopes in sediments during Period I (before ~470 CE) in this study, while the red-filled circles represent the Hg isotopes in sediments during Period II (after ~470 CE). “ZSS PHg” represents the atmospheric particulate Hg at Zhongshan Station⁵¹, while “GWS TGM” represents atmospheric total gaseous Hg at Great Wall Station in Antarctica⁵². “Antarctic sediment” represents the coastal sediments of King George Island, Antarctica⁶². The black arrow in subpanel (b) indicates a shift in the depth of occurrence of North Pacific fish from 200 m to 600 m²⁵. Literature for Hg isotope data for other samples can be found in Supplementary Table 2.

process, for the reasons outlined below. First, the Hg species in the food sources of southern elephant seals are dominated by MeHg. According to the dietary analysis of southern elephant seals (details in Supplementary Note 1), cephalopods and fish are the main foods of southern elephant seals, and the Hg in both preys is dominated by MeHg (average above ~80% of total Hg)^{62,79,80}. Thus, the fraction of inorganic Hg(II) directly contributed by the food sources should be small. Although a recent analysis showed a relatively low MeHg content in seal feces (average below ~20% of total Hg)⁸¹, the proportion of Hg(II) in sediments or in seal feces is not equivalent to the proportion of

Hg(II) in the food sources ingested by seals, because seals have a strong ability to detoxify MeHg by converting it to Hg(II) in the liver and excreting Hg(II)^{20,81,82}. Since biological metabolic processes do not produce Hg MIF^{20,21,25–27}, the inorganic Hg(II) converted from MeHg via *in vivo* demethylation should inherit the odd-MIF value of the MeHg from food. Therefore, it is more likely that the inorganic Hg(II) in seal feces was mostly converted from MeHg in the food sources, and thus it is reasonable to assume that the $\Delta^{199}\text{Hg}$ in seal feces mainly reflects the $\Delta^{199}\text{Hg}$ of MeHg in the food sources, which primarily originated from photodemethylation in the marine environment.

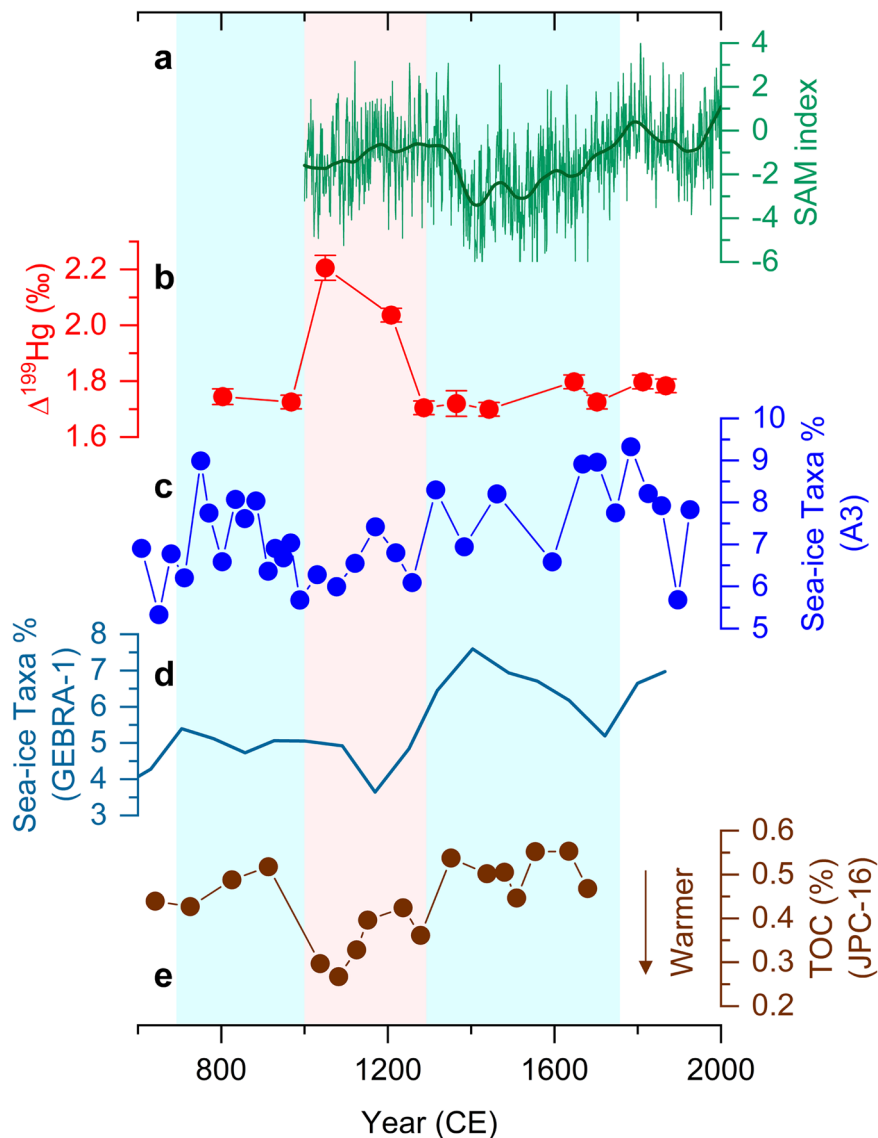


Fig. 4 Past climate change and the Hg cycling. **a** The Southern Annular Mode (SAM) index is plotted according to Abram et al.⁸⁸, and the dark green line represents the result of “LOWESS” smoothing. **b** Variation of $\Delta^{199}\text{Hg}$ in the HF4 sediments after ~750 CE. **(c), (d)** Changes in the proportion of sea-ice taxa diatoms in the A3 and GEBRA-1 cores^{103,104}. **e** Changes in total organic carbon (TOC) content in the JPC-16 sedimentary column, indicative of past climate change⁷². Error bars for $\Delta^{199}\text{Hg}$ represent analytical uncertainty (2σ , see “Methods” for details). The light red shaded area represents the warm climate period, while the light blue shaded areas represent the cold climate periods.

Second, the ratio or regression slope between $\Delta^{199}\text{Hg}$ and $\Delta^{201}\text{Hg}$ is an important indicator of photochemical processes^{22,23}. Experimental studies have shown that aqueous photodegradation of MeHg and photoreduction of Hg(II) yield $\Delta^{199}\text{Hg}/\Delta^{201}\text{Hg}$ slopes of ~1.3 and ~1.0, respectively^{23,24}. The slope between $\Delta^{199}\text{Hg}$ and $\Delta^{201}\text{Hg}$ in our sediment samples is ~1.17 (Supplementary Fig. 4). This slope is similar to Zheng et al.²⁸, who also found a $\Delta^{199}\text{Hg}/\Delta^{201}\text{Hg}$ slope between 1.0 and 1.3 (~1.11) in biological sediments dominated by seal feces on Ross Island, and argued that the intermediate $\Delta^{199}\text{Hg}/\Delta^{201}\text{Hg}$ slope reflects a combination of residual MeHg that sank from the surface ocean (which should carry a signal of photodemethylation with a $\Delta^{199}\text{Hg}/\Delta^{201}\text{Hg}$ slope of ~1.3) and MeHg produced by in situ microbial methylation in intermediate waters (which should maintain the odd-MIF signal of Hg(II) at surface ocean with a $\Delta^{199}\text{Hg}/\Delta^{201}\text{Hg}$ slope of ~1.0). However, the $\Delta^{199}\text{Hg}/\Delta^{201}\text{Hg}$ slope of our sediment samples is close to the value compiled from global marine fish (~1.2)^{15,23,25,67,83,84}, which is probably more representative of the $\Delta^{199}\text{Hg}/\Delta^{201}\text{Hg}$ slope of MeHg

photodegradation in actual seawater. Moreover, the $\Delta^{199}\text{Hg}$ values of the total Hg in global open ocean surface seawater, which is dominated by inorganic Hg(II), are typically less than ~0.4‰⁵⁰. These $\Delta^{199}\text{Hg}$ values are too low to explain the much higher $\Delta^{199}\text{Hg}$ values in the seal-feces-dominated sediments (1.81‰ in average after ~750 CE). Therefore, the odd-MIF in the seal-feces-dominated sediments should be primarily produced by the photodemethylation process in seawater.

Seal-derived Hg MIF records changes in sea ice conditions.

Following the argument in Section 2.2, the increase of $\Delta^{199}\text{Hg}$ between ~1000 and ~1300 CE in period II (corresponding to the MCA) is most likely linked to the change of MeHg $\Delta^{199}\text{Hg}$ values in seawater, which can be caused by a change in the source of MeHg to seawater or in the degree of marine photodemethylation.

The sources of Hg in seawater in the study area may include snow and ice melt input, upwelling (intrusion of Circumpolar Deep Water, CDW), and atmospheric deposition. Snow/ice melt in polar

regions is supposed to have strongly negative $\Delta^{199}\text{Hg}$ (as low as -5‰) produced by photoreduction on snow/ice surface as shown by both experiments and direct measurements of polar snow samples^{4,53,54}. Thus, during the MCA (~1000 CE to ~1300 CE), the more frequent ice and snow melting events are supposed to lower the $\Delta^{199}\text{Hg}$ value of marine MeHg, which is inconsistent with the elevated $\Delta^{199}\text{Hg}$ in sediments during MCA (Fig. 4), suggesting that enhanced snow/ice melting is not the main reason for the increase of $\Delta^{199}\text{Hg}$ during MCA. Furthermore, the higher Southern Annular Mode index (SAM; the dominant atmospheric circulation mode in the Southern Hemisphere) during the MCA indicates an intensification of westerly winds and therefore stronger upwelling in the study area (Fig. 4)^{85–88}. However, stronger upwelling is expected to bring MeHg with lower $\Delta^{199}\text{Hg}$ from deeper seawater, which also cannot explain the increase of $\Delta^{199}\text{Hg}$ during MCA. At last, the change in atmospheric deposition to ocean could potentially change the initial $\Delta^{199}\text{Hg}$ of MeHg before undergoing photodegradation in seawater. Thus, there may be a possibility that the increase of $\Delta^{199}\text{Hg}$ during MCA was due to an increase of the initial $\Delta^{199}\text{Hg}$ of atmospheric deposition. However, there is no evidence for a sudden change of atmospheric deposition during MCA. Although large variations of temperatures (up to about 12 °C) have been found to affect atmospheric deposition of Hg to snow in East Antarctica (Dome C)^{89,90}, the difference in temperature between MCA and LIA in the Antarctic Peninsula may be within 0.4 degrees⁹¹. Thus, the possibility that the increase of $\Delta^{199}\text{Hg}$ during MCA was due to changes in atmospheric Hg deposition to ocean is very low.

We suggest that the increase of $\Delta^{199}\text{Hg}$ during MCA mainly reflects the enhanced MeHg photodemethylation in seawater caused by decreased sea ice extent. During the MCA (i.e., ~1000–1300 CE), the decreased sea ice extent can facilitate penetration of solar radiation into seawater, which could enhance the photodegradation of MeHg in seawater, and thus increase the $\Delta^{199}\text{Hg}$ in the residual MeHg (Fig. 4). As MeHg enters the food chain, the $\Delta^{199}\text{Hg}$ in seals inherits that of the residual MeHg in seawater, which is eventually recorded in our sediment samples. On the contrary, more sea ice coverage may have inhibited MeHg photodegradation during both cold periods (i.e., ~750–1000 CE and ~1300–1750 CE), leading to lower $\Delta^{199}\text{Hg}$ in sediments. The effect of sea ice on the photodegradation of marine MeHg has been reported before. Point et al.²¹ estimated that $\Delta^{199}\text{Hg}$ in murre eggs increased by ~0.68‰ when moving from the 90% ice-covered Cape Lisburne colony to the 0% ice-covered Gulf of Alaska colonies, corresponding to a ~8% increase in the degree of photodemethylation. By analogy, our sediment samples show a difference of 0.39‰ in $\Delta^{199}\text{Hg}$ between the cold and warm periods, which could account for roughly a 52% difference in sea ice coverage and a 5% difference in the degree of photodemethylation between warm and cold periods.

Our finding of increased $\Delta^{199}\text{Hg}$ in biological sediments due to enhanced photodemethylation in the Antarctic marine environment is comparable to the study by Zheng et al.²⁸, who also found a similar degree of $\Delta^{199}\text{Hg}$ increase by about 0.4‰ from ~1490 CE to ~1650 CE in another sediment core (MB6) strongly influenced by the Adélie penguin on Ross Island, Antarctica. However, the timing of the $\Delta^{199}\text{Hg}$ increase is different between our study and Zheng et al.²⁸ (Fig. 4). We suggest that this difference may be largely related to differences in regional climate and environment. One of the important differences between the two regions is that the Ross Sea coast is strongly affected by katabatic winds^{92,93}, and large coastal polynyas exist in the Ross Sea area⁹⁴. In contrast, the Fildes Peninsula area is less affected by katabatic winds and lacks large coastal polynyas. Thus, the colder climate and more sea ice from ~1490 CE to 1650 CE in the Fildes Peninsula area would result in decreased MeHg photodegradation, leading to the lower

$\Delta^{199}\text{Hg}$ in sediments of this study (Fig. 4). However, during the same period, stronger katabatic winds and enhanced upwelling in the Ross Sea area would have increased coastal polynyas^{28,95,96}, which may have promoted MeHg photodemethylation and hence the increase of $\Delta^{199}\text{Hg}$ in sediments (MB6) on Ross Island²⁸.

Modern climate warming and sea ice loss in the Antarctic Peninsula region are expected to further enhance MeHg photodegradation in seawater, and thus further increase $\Delta^{199}\text{Hg}$. There is indeed a weak increasing trend of $\Delta^{199}\text{Hg}$ approaching the modern times after MCA (Fig. 4). However, the resolution of the current sediment core is not sufficient to resolve the modern changes. Two modern elephant seal feces samples collected from Byers peninsula and Zhongshan Station show lower $\Delta^{199}\text{Hg}$ than sediments during the cold periods (Fig. 3)²⁸. This may be related to differences in sampling locations and the individual variation of seals. Differences in regional atmospheric and marine environments (e.g., sea ice coverage) may cause large differences in $\Delta^{199}\text{Hg}$ in seals. Moreover, each sediment sample in the study core represents seal feces input over a long time period, whereas fresh seal feces samples tend to be the excrement of individual seals, and there may be large variations in Hg isotope compositions among individuals (see more details in Supplementary Note 2).

Antarctica is a hotspot of climate change and studying the historical changes in Hg sources and processes will provide important insights for the future changes in Hg cycle under global warming. Using Hg MIF values from a sedimentary column strongly influenced by seal feces input, we reconstructed the change in the degree of photodemethylation in seawater in the study area over the past ~1200 years. The temporal variation of $\Delta^{199}\text{Hg}$ in sediments during the historical period suggests that sea ice coverage has a substantial influence on the photodegradation of marine MeHg, which is consistent with the conclusions of previous Hg isotope studies in modern Arctic biological samples^{20,21}. From another perspective, our study also demonstrates that Hg isotopes in biological sediments are valuable proxies of past climate change. The ice-free area of Antarctica is rich in biological sediments, which can provide valuable records for studying the temporal and spatial changes of the marine MeHg cycle in historical periods. However, the current work cannot answer whether this change in the degree of photodemethylation can substantially affect Hg levels in organisms, which are likely affected by multiple factors such as primary productivity, trophic levels, and associated atmospheric and oceanic processes. Further research is needed in the future to better understand this complex biogeochemical system. Moreover, Hg isotopes in modern biological samples or biological sediment cores with better temporal resolution may provide more details about the relationship between sea ice and marine Hg cycling across different time periods, and thus warrant further investigation.

Methods

Site description and sample collection. During the Eighteenth Chinese Antarctic Research Expedition (November 2001–March 2002), a 42.5 cm long sediment core, referred to as HF4, was obtained from a terrestrial catchment (62°11'57"S, 59°58'48"W) in a depositional basin situated on the west coast of Fildes Peninsula³⁹. This basin is located within the second marine terrace at an altitude of 8 m (see Fig. 1 and Supplementary Fig. 1). The seals inhabiting around the sampling site were identified as southern elephant seals (*Mirounga leonina*)³⁹. During sampling, a 12 cm diameter PVC plastic gravity corer was inserted vertically until bedrock was encountered and extracted rapidly. The sediment core was divided into sections in the laboratory, with an interval of 0.5 cm for the top 18 cm and 1.0 cm for the rest of the sediment. There was a substantial quantity of seal hair in the top 18 cm of sediment, whereas the subsequent 5 cm of sediment exhibited a minimal presence of seal hair. No seal hair was found in the sediment below 23 cm. Each section was air-dried and thoroughly mixed. Approximately one-eighth of each bulk sub-sample was further dried for 24 hours at 105°C, and then used to count seal hairs using the methodology described by Hodgson et al.⁹⁷ The dating of the HF4 core is determined using ¹³⁷Cs and conventional ¹⁴C dating methods, as

reported in previous studies^{39,40}. In order to mitigate the marine reservoir effect on ¹⁴C dating, only four sediment samples with minimal presence of seal hairs were selected (Supplementary Table 3). By performing a linear extrapolation of ¹⁴C-age against depth, an intercept value of 114 years was obtained for the modern surface sediments (confirmed by ¹³⁷Cs activities)^{39,40} (Supplementary Fig. 5a). Hence, the value of 114 years is considered to account for the reservoir effect, and used to correct the measured radiocarbon ages by subtracting this value from them. The chronology of the core was established by applying linear interpolation between the corrected ¹⁴C ages (Supplementary Fig. 5b).

Hg stable isotope measurements. The determination for Hg concentration in sediments and quality control have been reported in previous work^{39,40}. Prior to isotope analysis, Hg in samples was first extracted using a thermal combustion method⁹⁸. Briefly, powdered samples (typically <2 g) were combusted within the furnace unit of Hydra IIC Direct Mercury Analyzer at 800 °C under an oxygen flow of 250 ml min⁻¹. The elemental mercury vapor released during thermal decomposition was swept into a trapping solution comprising 0.2% KMnO₄ (w/w) and 5% H₂SO₄ (v/v), where it was oxidized to Hg(II). To monitor Hg yields and the precision of Hg isotope measurement, procedural blanks were processed alongside samples, as was standard reference material (CCRMP TILL-1, Ontario soils). Recoveries of Hg for the procedure standard were 96.1 ± 2% (1 SD, n = 3). Recoveries of Hg for all samples were 94.4 ± 8% (1 SD, n = 24). Mercury concentrations in procedural blanks were typically <0.04 ng g⁻¹, which is less than 1% of the Hg present in samples.

Mercury isotopes were analyzed via multi-collector inductively coupled plasma mass spectrometry (MC-ICP-MS, Neptune Plus, Thermo Scientific) at University of Toronto using previously described techniques^{98,99}. The trapping solutions containing Hg extracted from samples were first neutralized with NH₂OH·HCl to reduce KMnO₄, and then diluted to 1–2 ng g⁻¹ Hg using a matrix matched pre-neutralized trapping solution. The Hg in the diluted solutions was introduced into the instrument using the online cold vapor generation method⁹⁹. Instrumental mass bias was corrected using the ²⁰⁵Tl/²⁰³Tl ratio of an internal Tl standard (NIST 997) introduced as desolvated aerosol and strict standard-sample-standard bracketing with the Hg standard reference material (SRM) NIST SRM 3133. The bracketing standard was prepared in the same matrix solution as samples and concentrations were matched such that standard signal sizes were matched to within ±10% of sample signal sizes. Isobaric interference from ²⁰⁴Pb was corrected by measuring ²⁰⁶Pb, but was always negligible. On-peak zero corrections determined from a matrix matched blank run prior to the sample were applied to all Hg and Pb masses. Mercury isotope compositions are reported using δ notation:

$$\delta^x\text{Hg}(\text{‰}) = \left[\frac{(^x\text{Hg}/^{198}\text{Hg})_{\text{sample}}}{(^x\text{Hg}/^{198}\text{Hg})_{\text{NIST3133}}} - 1 \right] \times 1000 \quad (1)$$

where x is the mass number of each Hg isotope, including 199, 200, 201, 202 and 204. MDF is reported as δ²⁰²Hg. MIF (Δ^xHg) is reported as the difference between measured δ^xHg and the theoretical values based on kinetic mass dependent fractionation law¹⁰⁰:

$$\Delta^x\text{Hg} = \delta^x\text{Hg} - \beta \times \delta^{202}\text{Hg} \quad (2)$$

where x is the mass number 199, 200, 201 and 204. β is a scaling constant to estimate the theoretical kinetic MDF, and it is 0.2520, 0.5024, 0.7520 and 1.4930 for ¹⁹⁹Hg, ²⁰⁰Hg, ²⁰¹Hg and ²⁰⁴Hg, respectively. Each sample was measured twice and an in-house Hg standard JTBaker was measured 5–7 times during each session. The analytical uncertainties (2σ) are reported as either 2 standard error (2SE) of sample replicates or 2 standard deviation (2SD) of JTBaker (Supplementary Table 1 and 4), whichever is higher. The measured Hg isotope ratios for JTBaker (δ²⁰²Hg = -0.63 ± 0.05‰; Δ¹⁹⁹Hg = 0.02 ± 0.02‰; Δ²⁰⁰Hg = 0.01 ± 0.03‰, n = 12) and for TILL-1 (δ²⁰²Hg = -1.11 ± 0.01‰; Δ¹⁹⁹Hg = -0.11 ± 0.01‰; Δ²⁰⁰Hg = 0.01 ± 0.01‰, n = 3) are both consistent with published values^{98,101}.

Reporting summary. Further information on research design is available in the Nature Portfolio Reporting Summary linked to this article.

Data availability

The datasets used in this study and source data for graphs and charts will be available from figshare (<https://doi.org/10.6084/m9.figshare.23552385.v2>). Sea ice data for the Antarctic are available from Met Office Hadley Center observations datasets¹⁰² (<https://www.metoffice.gov.uk/hadobs/hadist/data/download.html>). The Southern Annular Mode (SAM) index⁹⁸ is obtained from <https://www.ncei.noaa.gov/access/paleo-search/>, and can also be downloaded from figshare (<https://doi.org/10.6084/m9.figshare.23552385.v2>).

Code availability

The codes used for this study are now accessible to the public via GitHub (<https://github.com/lhw21/codes-for-seal-affected-sediments-Hg-isotopes>).

Received: 20 September 2022; Accepted: 6 July 2023;

Published online: 14 July 2023

References

- Lyman, S. N., Cheng, I., Gratz, L. E., Weiss-Penzias, P. & Zhang, L. An updated review of atmospheric mercury. *Sci. Total Environ.* **707**, <https://doi.org/10.1016/j.scitotenv.2019.135575> (2020).
- Cossa, D. et al. Mercury in the Southern Ocean. *Geochimica Et Cosmochimica Acta* **75**, 4037–4052 (2011).
- Yue, F., Xie, Z., Yan, J., Zhang, Y. & Jiang, B. Spatial Distribution of Atmospheric Mercury Species in the Southern Ocean. *J. Geophys. Res.-Atmos.* **126**, <https://doi.org/10.1029/2021jd034651> (2021).
- Sherman, L. S. et al. Mass-independent fractionation of mercury isotopes in Arctic snow driven by sunlight. *Nat. Geosci.* **3**, 173–177 (2010).
- Costa, M. & Liss, P. S. Photoreduction of mercury in sea water and its possible implications for Hg-0 air-sea fluxes. *Marine Chem.* **68**, 87–95 (1999).
- Poulain, A. J. et al. Redox transformations of mercury in an Arctic snowpack at springtime. *Atmos. Environ.* **38**, 6763–6774 (2004).
- Cossa, D., Averty, B. & Pirrone, N. The origin of methylmercury in open Mediterranean waters. *Limnol. Oceanogr.* **54**, 837–844 (2009).
- Sunderland, E. M., Krabbenhoft, D. P., Moreau, J. W., Strode, S. A. & Landing, W. M. Mercury sources, distribution, and bioavailability in the North Pacific Ocean: Insights from data and models. *Global Biogeochem. Cycles* **23**, <https://doi.org/10.1029/2008gb003425> (2009).
- Monperrus, M. et al. Mercury methylation, demethylation and reduction rates in coastal and marine surface waters of the Mediterranean Sea. *Marine Chem.* **107**, 49–63 (2007).
- Munson, K. M., Lamborg, C. H., Boiteau, R. M. & Saito, M. A. Dynamic mercury methylation and demethylation in oligotrophic marine water. *Biogeochemistry* **15**, 6451–6460 (2018).
- Cherel, Y. et al. Accumulate or eliminate? Seasonal mercury dynamics in albatrosses, the most contaminated family of birds. *Environ. Pollut.* **241**, 124–135 (2018).
- Heimbueger, L.-E. et al. Methyl mercury distributions in relation to the presence of nano- and picophytoplankton in an oceanic water column (Ligurian Sea, North-western Mediterranean). *Geochimica Et Cosmochimica Acta* **74**, 5549–5559 (2010).
- Mason, R. P. et al. Mercury biogeochemical cycling in the ocean and policy implications. *Environ. Res.* **119**, 101–117 (2012).
- Sellers, P., Kelly, C. A., Rudd, J. W. M. & MacHutchon, A. R. Photodegradation of methylmercury in lakes. *Nature* **380**, 694–697 (1996).
- Motta, L. C., Blum, J. D., Popp, B. N., Drazen, J. C. & Close, H. G. Mercury stable isotopes in flying fish as a monitor of photochemical degradation of methylmercury in the Atlantic and Pacific Oceans. *Marine Chem.* **223**, <https://doi.org/10.1016/j.marchem.2020.103790> (2020).
- DiMento, B. P. & Mason, R. P. Factors controlling the photochemical degradation of methylmercury in coastal and oceanic waters. *Marine Chem.* **196**, 116–125 (2017).
- Black, F. J., Poulin, B. A. & Flegal, A. R. Factors controlling the abiotic photodegradation of monomethylmercury in surface waters. *Geochimica Et Cosmochimica Acta* **84**, 492–507 (2012).
- Lehnher, I. & Louis, V. L. S. Importance of ultraviolet radiation in the photodemethylation of methylmercury in freshwater ecosystems. *Environ. Sci. Technol.* **43**, 5692–5698 (2009).
- Hammerschmidt, C. R. & Fitzgerald, W. F. Photodecomposition of methylmercury in an arctic Alaskan lake. *Environ. Sci. Technol.* **40**, 1212–1216 (2006).
- Masbou, J. et al. Hg stable isotope time trend in ringed seals registers decreasing sea ice cover in the Alaskan Arctic. *Environ. Sci. Technol.* **49**, 8977–8985 (2015).
- Point, D. et al. Methylmercury photodegradation influenced by sea-ice cover in Arctic marine ecosystems. *Nat. Geosci.* **4**, 188–194 (2011).
- Tsui, M. T.-K., Blum, J. D. & Kwon, S. Y. Review of stable mercury isotopes in ecology and biogeochemistry. *Sci. Total Environ.* **716**, <https://doi.org/10.1016/j.scitotenv.2019.135386> (2020).
- Blum, J. D., Sherman, L. S. & Johnson, M. W. Mercury isotopes in earth and environmental sciences. *Ann. Rev. Earth Planet. Sci.* **42**, 249–269 (2014).
- Bergquist, B. A. & Blum, J. D. Mass-dependent and -independent fractionation of Hg isotopes by photoreduction in aquatic systems. *Science* **318**, 417–420 (2007).
- Blum, J. D., Popp, B. N., Drazen, J. C., Choy, C. A. & Johnson, M. W. Methylmercury production below the mixed layer in the North Pacific Ocean. *Nat. Geosci.* **6**, 879–884 (2013).
- Blum, J. D. et al. Mercury isotopes identify near-surface marine mercury in deep-sea trench biota. *Proc. Natl. Acad. Sci. USA* **117**, 29292–29298 (2020).

27. Sun, R. et al. Methylmercury produced in upper oceans accumulates in deep Mariana Trench fauna. *Nat. Commun.* **11**, <https://doi.org/10.1038/s41467-020-17045-3> (2020).
28. Zheng, W., Xie, Z. & Bergquist, B. A. Mercury stable isotopes in ornithogenic deposits as tracers of historical cycling of Mercury in Ross Sea, Antarctica. *Environ. Sci. Technol.* **49**, 7623–7632 (2015).
29. Turner, J. et al. Antarctic climate change and the environment: an update. *Polar Record* **50**, 237–259 (2014).
30. Turner, J. et al. Absence of 21st century warming on Antarctic Peninsula consistent with natural variability. *Nature* **535**, 411–+ (2016).
31. Oliva, M. et al. Recent regional climate cooling on the Antarctic Peninsula and associated impacts on the cryosphere. *Sci. Total Environ.* **580**, 210–223 (2017).
32. Turner, J. et al. Antarctic temperature variability and change from station data. *Int. J. Climatol.* **40**, 2986–3007 (2020).
33. Silva, A. B. et al. Spatial and temporal analysis of changes in the glaciers of the Antarctic Peninsula. *Global Planetary Change* **184**, <https://doi.org/10.1016/j.gloplacha.2019.103079> (2020).
34. Goosse, H. & Zunz, V. Decadal trends in the Antarctic sea ice extent ultimately controlled by ice-ocean feedback. *Cryosphere* **8**, 453–470 (2014).
35. Li, X., Holland, D. M., Gerber, E. P. & Yoo, C. Impacts of the north and tropical Atlantic Ocean on the Antarctic Peninsula and sea ice. *Nature* **505**, 538–+ (2014).
36. Turner, J. et al. Recent decrease of summer sea ice in the Weddell Sea, Antarctica. *Geophys. Res. Lett.* **47**, <https://doi.org/10.1029/2020gl087127> (2020).
37. Sun, L. G., Xie, Z. Q. & Zhao, J. L. Palaeoecology - A 3,000-year record of penguin populations. *Nature* **407**, 858–858 (2000).
38. Yang, L. et al. Enhanced westerlies drove penguin movement at 1000 yr BP on Ardley Island, west Antarctic Peninsula. *Quaternary Sci. Rev.* **214**, 44–53 (2019).
39. Sun, L. G. et al. A 1,500-year record of Antarctic seal populations in response to climate change. *Polar Biology* **27**, 495–501 (2004).
40. Sun, L. et al. A 2000-year record of mercury and ancient civilizations in seal hairs from King George Island, West Antarctica. *Sci. Total Environ.* **368**, 236–247 (2006).
41. Braun, C., Mustafa, O., Nordt, A., Pfeiffer, S. & Peter, H.-U. Environmental monitoring and management proposals for the Fildes Region, King George Island, Antarctica. *Polar Res.* **31**, <https://doi.org/10.3402/polar.v31i0.18206> (2012).
42. Hans-Ulrich, P. et al. *The current environmental situation and proposals for the management of the Fildes Peninsula Region*. 127–128 (Federal Environment Agency, 2013).
43. Amaro, E. et al. Assessing trace element contamination in Fildes Peninsula (King George Island) and Ardley Island, Antarctic. *Marine Pollut. Bulletin* **97**, 523–527 (2015).
44. Bartov, G. et al. Environmental impacts of the Tennessee Valley Authority Kingston Coal Ash Spill. 1. Source apportionment using mercury stable isotopes. *Environ. Sci. Technol.* **47**, 2092–2099 (2013).
45. Donovan, P. M. et al. Identification of multiple mercury sources to stream Sediments near Oak Ridge, TN, USA. *Environ. Sci. Technol.* **48**, 3666–3674 (2014).
46. Dong, W., Bian, Y., Liang, L. & Gu, B. Binding constants of mercury and dissolved organic matter determined by a modified ion exchange technique. *Environ. Sci. Technol.* **45**, 3576–3583 (2011).
47. Haitzer, M., Aiken, G. R. & Ryan, J. N. Binding of mercury(II) to aquatic humic substances: Influence of pH and source of humic substances. *Environ. Sci. Technol.* **37**, 2436–2441 (2003).
48. Moynier, F. et al. The mercury isotopic composition of earth's mantle and the use of mass independently fractionated Hg to test for recycled crust. *Geophys. Res. Lett.* **48**, <https://doi.org/10.1029/2021gl094301> (2021).
49. Ogrinc, N., Hintelmann, H., Kotnik, J., Horvat, M. & Pirrone, N. Sources of mercury in deep-sea sediments of the Mediterranean Sea as revealed by mercury stable isotopes. *Sci. Rep.* **9**, <https://doi.org/10.1038/s41598-019-48061-z> (2019).
50. Jiskra, M. et al. Mercury stable isotopes constrain atmospheric sources to the ocean. *Nature* **597**, 678–+ (2021).
51. Li, C. et al. Seasonal variation of mercury and its isotopes in atmospheric particles at the Coastal Zhongshan Station, Eastern Antarctica. *Environ. Sci. Technol.* **54**, 11344–11355 (2020).
52. Yu, B. et al. Katabatic wind and sea-ice dynamics drive isotopic variations of total gaseous mercury on the Antarctic Coast. *Environ. Sci. Technol.* **55**, 6449–6458 (2021).
53. Zheng, W. et al. Mercury stable isotopes reveal the sources and transformations of atmospheric Hg in the high Arctic. *Appl. Geochem.* **131**, <https://doi.org/10.1016/j.apgeochem.2021.105002> (2021).
54. Douglas, T. A. & Blum, J. D. Mercury isotopes reveal atmospheric gaseous mercury deposition directly to the Arctic Coastal Snowpack. *Environ. Sci. Technol. Lett.* **6**, 235–242 (2019).
55. Sherman, L. S. et al. Mercury isotopic composition of hydrothermal systems in the Yellowstone Plateau volcanic field and Guaymas Basin sea-floor rift. *Earth Planet. Sci. Lett.* **279**, 86–96 (2009).
56. Zambardi, T., Sonke, J. E., Toutain, J. P., Sortino, F. & Shinohara, H. Mercury emissions and stable isotopic compositions at Vulcano Island (Italy). *Earth Planet. Sci. Lett.* **277**, 236–243 (2009).
57. Smith, C. N., Kesler, S. E., Blum, J. D. & Rytuba, J. J. Isotope geochemistry of mercury in source rocks, mineral deposits and spring deposits of the California Coast Ranges, USA. *Earth Planet. Sci. Lett.* **269**, 398–406 (2008).
58. Demers, J. D., Blum, J. D. & Zak, D. R. Mercury isotopes in a forested ecosystem: Implications for air-surface exchange dynamics and the global mercury cycle. *Global Biogeochem. Cycles* **27**, 222–238 (2013).
59. Obrist, D. et al. Tundra uptake of atmospheric elemental mercury drives Arctic mercury pollution. *Nature* **547**, 201–+ (2017).
60. Liu, H., Yu, B., Shi, J., Zhang, Q. & Jiang, G. Comparison of two pretreatment methods for mercury stable isotope analysis in Antarctic moss. *Adv. Polar Sci.* **028**, 75–80 (2017).
61. Zhang, H. et al. Atmospheric mercury inputs in montane soils increase with elevation: evidence from mercury isotope signatures. *Sci. Rep.* **3**, <https://doi.org/10.1038/srep03322> (2013).
62. Liu, H. et al. Different circulation history of mercury in aquatic biota from King George Island of the Antarctic. *Environ. Pollut.* **250**, 892–897 (2019).
63. Biswas, A., Blum, J. D., Bergquist, B. A., Keeler, G. J. & Xie, Z. Natural mercury isotope variation in coal deposits and organic soils. *Environ. Sci. Technol.* **42**, 8303–8309 (2008).
64. Kwon, S. Y. et al. Absence of fractionation of mercury isotopes during trophic transfer of methylmercury to freshwater fish in captivity. *Environ. Sci. Technol.* **46**, 7527–7534 (2012).
65. Day, R. D. et al. Mercury stable isotopes in seabird eggs reflect a gradient from terrestrial geogenic to oceanic mercury reservoirs. *Environ. Sci. Technol.* **46**, 5327–5335 (2012).
66. Perrot, V. et al. Tracing sources and bioaccumulation of mercury in Fish of Lake Baikal- Angara River using Hg isotopic composition. *Environ. Sci. Technol.* **44**, 8030–8037 (2010).
67. Madigan, D. J. et al. Mercury stable isotopes reveal influence of foraging depth on mercury concentrations and Growth in Pacific Bluefin Tuna. *Environ. Sci. Technol.* **52**, 6256–6264 (2018).
68. Li, M. et al. Selenium and stable mercury isotopes provide new insights into mercury toxicokinetics in pilot whales. *Sci. Total Environ.* **710**, <https://doi.org/10.1016/j.scitotenv.2019.136325> (2020).
69. Hall, B. L. Late-Holocene advance of the Collins Ice Cap, King George Island, South Shetland Islands. *Holocene* **17**, 1253–1258 (2007).
70. Hall, B. L. Holocene glacial history of Antarctica and the sub-Antarctic islands. *Quat. Sci. Rev.* **28**, 2213–2230 (2009).
71. Hall, B. L., Koffman, T. & Denton, G. H. Reduced ice extent on the western Antarctic Peninsula at 700–970 cal. yr BP. *Geology* **38**, 635–638 (2010).
72. Majewski, W., Wellner, J. S., Szczucinski, W. & Anderson, J. B. Holocene oceanographic and glacial changes recorded in Maxwell Bay, West Antarctica. *Marine Geology* **326**, 67–79 (2012).
73. Mayewski, P. A. et al. Holocene climate variability. *Quat. Res.* **62**, 243–255 (2004).
74. Monien, P., Schnetger, B., Brumsack, H.-J., Hass, H. C. & Kuhn, G. A geochemical record of late Holocene palaeoenvironmental changes at King George Island (maritime Antarctica). *Antarctic Sci.* **23**, 255–267 (2011).
75. Orsi, A. J., Cornuelle, B. D. & Severinghaus, J. P. Little Ice Age cold interval in West Antarctica: Evidence from borehole temperature at the West Antarctic Ice Sheet (WAIS) Divide. *Geophys. Res. Lett.* **39**, <https://doi.org/10.1029/2012gl051260> (2012).
76. Solomina, O. N. et al. Holocene glacier fluctuations. *Quat. Sci. Rev.* **111**, 9–34 (2015).
77. McIntyre, T. et al. Elephant seal dive behaviour is influenced by ocean temperature: implications for climate change impacts on an ocean predator. *Marine Ecology Progr. Ser.* **441**, 257–272 (2011).
78. Jaud, T., Dragon, A.-C., Garcia, J. V. & Guinet, C. Relationship between chlorophyll a concentration, light attenuation and diving depth of the Southern Elephant Seal *Mirounga leonina*. *Plos One* **7**, <https://doi.org/10.1371/journal.pone.0047444> (2012).
79. Seco, J. et al. Main drivers of mercury levels in Southern Ocean lantern fish *Myctophidae*. *Environ. Pollut.* **264**, <https://doi.org/10.1016/j.envpol.2020.114711> (2020).
80. Minet, A. et al. Mercury in the tissues of five cephalopods species: First data on the nervous system. *Sci. Total Environ.* **759**, <https://doi.org/10.1016/j.scitotenv.2020.143907> (2021).
81. Grajewska, A., Falkowska, L., Saniewska, D. & Pawliczka, I. Fur and faeces - Routes of mercury elimination in the Baltic grey seal (*Halichoerus grypus grypus*). *Sci. Total Environ.* **717**, <https://doi.org/10.1016/j.scitotenv.2020.137050> (2020).

82. Wagemann, R., Trebacz, E., Boila, G. & Lockhart, W. L. Mercury species in the liver of ringed seals. *Sci. Total Environ.* **261**, 21–32 (2000).
83. Senn, D. B. et al. Stable Isotope (N, C, Hg) Study of Methylmercury Sources and Trophic Transfer in the Northern Gulf of Mexico. *Environ. Sci. Technol.* **44**, 1630–1637 (2010).
84. Motta, L. C. et al. Mercury cycling in the north pacific subtropical gyre as revealed by mercury stable isotope ratios. *Global Biogeochem. Cycles* **33**, 777–794 (2019).
85. Thompson, D. W. J. et al. Signatures of the Antarctic ozone hole in Southern Hemisphere surface climate change. *Nat. Geosci.* **4**, 741–749 (2011).
86. Stammerjohn, S. E., Martinson, D. G., Smith, R. C., Yuan, X. & Rind, D. Trends in Antarctic annual sea ice retreat and advance and their relation to El Niño–Southern Oscillation and Southern Annular Mode variability. *J. Geophys. Res.-Oceans* **113**, <https://doi.org/10.1029/2007jc004269> (2008).
87. Martinson, D. G., Stammerjohn, S. E., Iannuzzi, R. A., Smith, R. C. & Vernet, M. Western Antarctic Peninsula physical oceanography and spatio-temporal variability. *Deep-Sea Res. Part II-Topical Stud. Oceanogr.* **55**, 1964–1987 (2008).
88. Abram, N. J. et al. Evolution of the Southern Annular Mode during the past millennium. *Nat. Clim. Change* **4**, 564–569 (2014).
89. Jitaru, P. et al. Atmospheric depletion of mercury over Antarctica during glacial periods. *Nat. Geosci.* **2**, 505–508 (2009).
90. Masson-Delmotte, V. et al. EPICA Dome C record of glacial and interglacial intensities. *Quat. Sci. Rev.* **29**, 113–128 (2010).
91. Silvestri, G., Laura Berman, A., De Vleeschouwer, F. & Wainer, I. Last millennium climate changes over the Antarctic Peninsula and southern Patagonia in CESM-LME simulations: Differences between Medieval Climate Anomaly and present-day temperatures. *Quat. Sci. Rev.* **274**, <https://doi.org/10.1016/j.quascirev.2021.107273> (2021).
92. Parish, T. R. & Bromwich, D. H. Continental-scale simulation of the antarctic katabatic wind regime. *J. Climate* **4**, 135–146 (1991).
93. Parish, T. R. & Cassano, J. J. The role of katabatic winds on the Antarctic surface wind regime. *Monthly Weather Rev.* **131**, 317–333 (2003).
94. Arrigo, K. R. & van Dijken, G. L. Phytoplankton dynamics within 37 Antarctic coastal polynya systems. *J. Geophys. Res.-Oceans* **108**, <https://doi.org/10.1029/2002jc001739> (2003).
95. Hu, Q.-H., Sun, L.-G., Xie, Z.-Q., Emslie, S. D. & Liu, X.-D. Increase in penguin populations during the Little Ice Age in the Ross Sea, Antarctica. *Sci. Rep.* **3**, <https://doi.org/10.1038/srep02472> (2013).
96. Yang, L. et al. Oceanographic mechanisms and penguin population increases during the Little Ice Age in the southern Ross Sea, Antarctica. *Earth Planet. Sci. Lett.* **481**, 136–142 (2018).
97. Hodgson, D. A., Johnston, N. M., Caulkett, A. P. & Jones, V. J. Palaeolimnology of Antarctic fur seal *Arctocephalus gazella* populations and implications for Antarctic management. *Biol. Conserv.* **83**, 145–154 (1998).
98. Zheng, W., Obrist, D., Weis, D. & Bergquist, B. A. Mercury isotope compositions across North American forests. *Global Biogeochem. Cycles* **30**, 1475–1492 (2016).
99. Shi, M. et al. The efficiency of Hg cold vapor generation and its influence on Hg isotope analysis by MC-ICP-MS. *J. Anal. Atomic Spectrometry* **38**, 1076–1087 (2023).
100. Blum, J. D. & Bergquist, B. A. Reporting of variations in the natural isotopic composition of mercury. *Anal. Bioanal. Chem.* **388**, 353–359 (2007).
101. Blum, J. D. & Johnson, M. W. Recent developments in mercury stable isotope analysis. *Non-Traditional Stable Isotopes* **82**, 733–757 (2017).
102. Rayner, N. A. et al. Global analyses of sea surface temperature, sea ice, and night marine air temperature since the late nineteenth century. *J. Geophys. Res.-Atmos.* **108**, <https://doi.org/10.1029/2002jd002670> (2003).
103. Barcena, M. A. et al. Record of Holocene glacial oscillations in Bransfield Basin as revealed by siliceous microfossil assemblages. *Antarctic Science* **10**, 269–285 (1998).
104. Barcena, M. A. et al. Holocene neoglacial events in the Bransfield Strait (Antarctica). Palaeoenvironmental and palaeoclimatic significance. *Scientia Marina* **70**, 607–619 (2006).

Acknowledgements

This study was funded by the National Natural Science Foundation of China (grant No. 41930532; 41973009). The authors thank the Chinese Arctic and Antarctic Administration for supporting the field campaign. The authors are grateful to Prof. R.B. Zhu and X.D. Liu for sample collection and analysis, and Dr. H. Li at University of Toronto for assistance in Hg isotope analysis. We especially thank Joel D. Blum for his critical comments and careful corrections on the manuscripts. Sample information are available at the Resource Sharing Platform of Polar Samples (<http://birds.chinare.org.cn>) maintained by Polar Research Institute of China (PRIC) and Chinese National Arctic & Antarctic Data Center (CN-NADC).

Author contributions

H.L.: Conceptualization, Formal analysis, Visualization, Writing—original draft, Writing—review & editing. W.Z.: Conceptualization, Sample analysis, Formal analysis, Funding acquisition, Supervision, Writing—review & editing. B.A.B.: Sample analysis, Formal analysis, Writing—review & editing. Y.G.: Formal analysis, Writing—review & editing. F.Y.: Formal analysis, Writing - review & editing. L.Y.: Formal analysis, Writing—review & editing. L.S.: Formal analysis, Resource, Writing—review & editing. Z.X.: Conceptualization, Formal analysis, Resource, Funding acquisition, Supervision, Writing—review & editing. Competing interests
The authors declare no competing interests.

Ethics

In the whole process of our research, including field investigation, sample collection, experimental analysis, data analysis, writing and other processes, all behaviors were in line with ethical standards, and did not cause any form of harm or adverse consequences to anyone and things.

Additional information

Supplementary information The online version contains supplementary material available at <https://doi.org/10.1038/s43247-023-00921-3>.

Correspondence and requests for materials should be addressed to Wang Zheng or Zhouqing Xie.

Peer review information *Communications Earth & Environment* thanks Maxime Enrico and the other, anonymous, reviewer(s) for their contribution to the peer review of this work. Primary Handling Editors: Sze Ling Ho and Clare Davis. A peer review file is available.

Reprints and permission information is available at <http://www.nature.com/reprints>

Publisher's note Springer Nature remains neutral with regard to jurisdictional claims in published maps and institutional affiliations.



Open Access This article is licensed under a Creative Commons Attribution 4.0 International License, which permits use, sharing, adaptation, distribution and reproduction in any medium or format, as long as you give appropriate credit to the original author(s) and the source, provide a link to the Creative Commons license, and indicate if changes were made. The images or other third party material in this article are included in the article's Creative Commons license, unless indicated otherwise in a credit line to the material. If material is not included in the article's Creative Commons license and your intended use is not permitted by statutory regulation or exceeds the permitted use, you will need to obtain permission directly from the copyright holder. To view a copy of this license, visit <http://creativecommons.org/licenses/by/4.0/>.

© The Author(s) 2023